

Silicon Carbide Nanoparticle-Filled Nanocomposites Using SLA Resin for Low Thermal Expansions

Muhammad Sufian*, Juan Rodriguez*, Kam Brown*, and Jitendra Tate*†

*Ingram School of Engineering, Texas State University, San Marcos, TX 78666

†Materials Science, Engineering and Commercialization Program, Texas State University, San Marcos, TX 78666

Abstract

Stereolithography (SLA) is a leading additive manufacturing technique favored for its high resolution and surface finish; however, its application in high-performance environments remains limited by the poor mechanical strength and high coefficient of thermal expansion (CTE) of standard photopolymer resins. In this study, a modified SLA resin system was developed by incorporating plasma-synthesized beta-phase silicon carbide (SiC) nanoparticles into a bisphenol A epoxy diacrylate (EBECRYL® 3700) matrix to enhance its mechanical and thermal properties. SiC was introduced at 0.5 wt% and 1 wt% concentrations, and its effects on microstructure, strength, stiffness, and thermal stability were evaluated. Scanning Electron Microscopy confirmed homogeneous dispersion of SiC at all loading levels, with only minor agglomeration at 1 wt%. Mechanical testing revealed that 1 wt% SiC improved tensile strength by over 80% (from 15.92 MPa to 28.82 MPa) and tensile modulus by 67% (from 342.1 MPa to 572.9 MPa) compared to the neat resin. Similarly, flexural strength increased from 17.20 MPa to 47.08 MPa, and flexural modulus from 298.3 MPa to 941.1 MPa. Thermomechanical analysis showed a substantial reduction in CTE, with the 0.5 wt% SiC formulation exhibiting the lowest thermal expansion. These results confirm the potential of SiC-reinforced SLA resins for thermally stable, mechanically robust applications in aerospace and precision component manufacturing.

Corresponding author: Dr. Jitendra S. Tate

*Email: jt31@txstate.edu, Phone: (737) 262-8010

1. INTRODUCTION

Stereolithography (SLA) is a versatile additive manufacturing (AM) technique that utilizes UV light to sequentially solidify liquid photopolymer resins layer by layer to create complex structures with great precision [1]. SLA has become standard practice across industries in engineering, healthcare, and dentistry as it is optimized for both smooth surface finishes and highly detailed components. Printing parameters such as layer thickness, exposure time, and post-processing techniques determine the final mechanical properties, precision, and accuracy of printed parts. While SLA is superior in resolution capabilities compared to most AM processes and has a good selection of compatible materials, parts often suffer from poor mechanical characteristics like shrinkage and brittleness, requiring additional post-processing as a result. Many research teams have shifted their focus to enhancing SLA technology and addressing issues that hinder the dimensional stability of parts for more demanding applications.

Since its inception in the 1980s, SLA has evolved significantly, transitioning through four distinct generations of innovation: scanning, projection, continuous, and volumetric stereolithography. Recent advancements in SLA technology have greatly improved its resolution, processing speed, and material compatibility for applications in biomedical engineering, microfluidics, and industrial manufacturing. SLA's capacity to produce intricate geometries with excellent surface finishes positions it as a premier AM technique. However, issues surrounding material limitations and necessary post-processing steps have provided room for expansion in areas of SLA research [2].

1.1 SLA Classification

Stereolithography (SLA) is a fundamental additive manufacturing (AM) technique categorized under vat photopolymerization, where liquid photopolymers are selectively solidified layer by layer using ultraviolet (UV) light exposure [3]. Within the broader AM landscape, SLA is grouped alongside material extrusion methods like fused deposition modeling (FDM) and powder bed fusion techniques such as selective laser sintering (SLS) and binder jetting. AM materials are classified by their physical states, either liquid, solid, or powder. While SLA stands out among the other AM techniques for its superior precision, surface finish, and relevance in high-precision applications, its reliance on photopolymers results in lower mechanical strength. While SLA excels in producing intricate and highly detailed components, the vat polymerization technique relies on specific types of materials that are prone to producing parts that lack adequate durability.

As a vat photopolymerization process, stereolithography utilizes UV light to solidify liquid resins into precise 3D structures. This classification differentiates from other additive manufacturing technologies such as material extrusion, which includes fused deposition modeling (FDM), and powder bed fusion methods like selective laser sintering (SLS) and binder jetting, each employing distinct material states and processing techniques. Pereira et al. (2019) systematically categorized 3D printing methods by evaluating research objectives and technical characteristics, highlighting SLA's superior resolution and surface quality. While SLA enables the fabrication of intricate designs with high accuracy, challenges persist with the high cost of resins and extensive post-processing requirements, limiting its material adaptability and scalability compared to extrusion and powder-based additive manufacturing techniques [4].

1.2 SLA Printing Process

Recent advancements in SLA research have expanded beyond conventional UV photoinitiators, introducing alternative polymerization techniques that improve material versatility and reduce costs. Kam et al. (2024) presented a novel SLA method utilizing thermal initiators (TIs) instead of traditional UV-based polymerization. Gold nanorods and silver nanoparticles were used as photothermal converters to facilitate localized polymerization through near-infrared (NIR) and visible light irradiation. By refining printing parameters such as initiator concentration, irradiation intensity, and thermal management, Kam et al. successfully developed a new method for SLA printing that supports both aqueous and non-aqueous environments, thereby addressing issues like the high cost of UV photo initiators and limited material selection. The study demonstrated the versatility of this approach for fabricating hydrogel and polymeric structures for applications such as bioprinting, drug delivery systems, and advanced polymer manufacturing [5].

1.3 Advantages of SLA

The development of the affordable SLA device showcases the significant advantages of SLA precision through the fabrication of microfluidic devices [6]. Compared to traditional CNC machining, SLA technology offers superior reproducibility while minimizing the need for manual post-processing. Furthermore, SLA enables the fabrication of complex internal fluidic channels that traditional manufacturing methods cannot achieve. This study demonstrates greater accessibility of microfluidic research through the creation of fine microchannels with commercially available SLA printing technology. The cost reduction and sustainability of SLA in this type of manufacturing application offer prototyping efficiency in biomedical research centered around complex microfluidic systems [6].

The pharmaceutical manufacturing industry has benefited from SLA's precise material control with the development of customizable drug delivery solutions [7]. Recent advancements in SLA technology have been applied in directly producing intricate geometries and specialized controlled-release drug formulations that traditional methods have been unable to achieve. This has positioned SLA as a particularly valuable candidate for producing personalized medicine. By facilitating multi-material structures, SLA can enhance drug bioavailability through the integration of multiple medications into a single dosage form, leading to improved therapeutic results for patients. Additionally, SLA's high-resolution and repeatability further establishes it as a tool for pharmaceutical research applications in tissue engineering and nanomedicine [7].

1.4 Solutions and Approach to Resin CTE Mismatch

1.4.1 Solutions for Material and Process Limitations

Micrometer-scale anisotropic inhomogeneities introduced during photopolymerization are defects in the SLA process that alter both the mechanical and chemical properties of printed structures [8]. To address this, Higgins et al (2021) integrated Digital Light Processing (DLP) technology with Atomic Force Microscopy (AFM), enabling the real-time analysis of the printing process at the voxel level. This method of approach provides detailed insights into resin behavior through in situ mechanical property mapping, nanoscale cure depth measurements, and dynamic rheological analysis. This method of approach provides detailed insights into resin behavior by capturing localized polymerization kinetics variations, this method enhances process optimization and improves fidelity of printed parts in both precision and structural consistency [8].

The functional performance of printed components often suffers from material contamination and limited compatibility in multimaterial SLA printing [9]. To address these issues, researchers have developed advanced resin switching and residual resin removal techniques, including centrifugal force-assisted material exchange, air jet cleaning, and vat-switching methods. Their findings demonstrate that centrifugal multimaterial (CM) 3D printing effectively reduces cross-contamination and enables the fabrication of high-resolution heterogeneous structures at larger scales. These advancements facilitate the precision fabrication of functionally graded SLA-printed parts, providing new applications in biomedical devices (Figure 1), soft robotics (Figure 2), and electronic components (Figure 3) [9].



Figure 1: Stereolithography 3D printed materials for bio-medical devices, soft-robotics and electronic components

Mubarak et al. (2020) explored nanoparticle-reinforced photopolymers as a solution to the mechanical fragility and thermal instability inherent in SLA-printed structures [10]. By incorporating annealed anatase TiO_2 nanoparticles (TNPs) into SLA resin, they achieved a 103% increase in tensile strength and a 32% improvement in elastic modulus compared to conventional SLA-printed samples. The annealing process enhanced the crystallinity of TiO_2 , strengthening polymer cross-links and improving UV light transmission, which in turn enhanced mechanical durability, thermal conductivity, and dimensional stability. Reinforcing SLA materials with nanoparticles provides a viable approach to mitigating material brittleness, expanding their applications in advanced engineering and medical device manufacturing [10].

1.4.2 Approach

Recent studies have shown that embedding nickel microparticles in photopolymer resins produces reinforced composites that increase the strength and structural integrity of SLA-printed components [11]. By optimizing mixing ratios, printing orientations, and turbidity stabilization, researchers introduced a slurry-based DLP printing technique that improved tensile strength and material uniformity. The study demonstrated that incorporating 6 wt% Ni resulted in a 75.5% increase in ultimate tensile strength and a 160% enhancement in strain capacity. Spectrophotometric and FTIR analysis verified resin-particle interactions, ensuring uniform dispersion and consistent curing. This nanoparticle-reinforced resin approach strengthens SLA materials, enhancing mechanical durability and structural consistency, which optimizes print fidelity for demanding applications [11].

Material constraints in SLA printing have led to extensive research on enhancing resin formulations and reinforcement strategies. To address SLA's mechanical and thermal limitations, researchers have incorporated fiber-reinforced composites with smart polymers, improving durability, flexibility, and resistance to environmental factors. Investigations into biocompatible and shape-memory resins have further expanded SLA's applications in biomedical engineering and industrial manufacturing. Additionally, research on additive manufacturing approaches such as powder bed fusion (PBF) and direct energy deposition (DED) has facilitated the fabrication of complex negative thermal expansion (NTE) structures. While these methods enable intricate geometries and multimaterial integration, challenges remain in optimizing material compatibility and interfacial bonding. Continued refinement of post-processing strategies and surface treatment methods aims to mitigate brittleness and improve mechanical performance, making SLA a more reliable option for high-precision applications [12].

1.5 Optimizing Resin for Thermal and Dimensional Stability

1.5.1 Importance of Thermal and Dimensional Stability

Ideal thermally stable SLA resins do not degrade, warp, or lose mechanical integrity when exposed to elevated temperatures. Dimensionally stable components retain their intended shape without excessive shrinkage, expansion, or distortion during curing and post-processing. Poor dimensional stability can lead to misalignment in assemblies, loss of tolerance, and mechanical failure. For applications such as nickel plating, where precise geometry is required to ensure even coating thickness and adhesion, resins must have low thermal expansion to prevent cracking and delamination. Optimizing SLA resin formulations with low thermal expansion additives and crosslinking agents enhances performance and broadens the range of viable applications for these materials [13].

The challenges associated with the thermal expansion and mechanical properties of SLA resins impact their application in harsh environments. Sharp temperature gradients, fluctuations, and divergence in CTE cause disproportionate expansion rates between SLA resins and their nickel plating. The CTE of nickel is approximately $13 \times 10^{-6} \mu\text{m}^\circ\text{C}^{-1}$, whereas commercially available SLA resins exhibit CTEs as high as $100 \times 10^{-6} \mu\text{m}^\circ\text{C}^{-1}$ [14]. This CTE mismatch is complicated by the poor tensile strength and brittleness typical of fully cured SLA resin components.

Investigations on the integration of nanomaterials in SLA resins, such as nanosilica and multi-walled carbon nanotubes, have shown that nanomaterial incorporation can offset the impact of temperature fluctuations by increasing the mechanical strength and rigidity of SLA resin. The improvements in mechanical and thermal characteristics in nanocomposite SLA resins translate to lowered CTEs by 25% for samples integrated with multi-walled carbon nanotubes and 36% for nanosilica [15].

The advantages of reduced CTEs in nanocomposite resins are presently counteracted by the complexities and secondary challenges associated with nanomaterials. Issues surrounding particle dispersion [16], agglomeration [17], viscosity of liquid resin [18], UV-light scattering [19] increased brittleness of highly-loaded samples [18] require careful consideration in selecting appropriate resin systems that work synergistically with nanomaterials in achieving mechanical and dimensional stability for dynamic high-temperature applications.

1.6 Nanocomposite Photopolymerization: UV Light Penetration, Scattering, Absorbance

Effective dispersion of nanomaterials like multi-walled carbon nanotube in resin can be achieved through mechanical mixing, ultrasonic methods, and the use of wetting and dispersing agents [18, 20]. When done properly, aggregation of the nanotubes is mitigated by reducing the surface tension of the resin [18]. One approach to preventing the microscopic clumping of nanotubes is the functionalization of their surfaces. This promotes interfacial bonding compatibility with the resin, adhesion, and mechanical load transfer [20]. When the viscosity of the resin is sufficiently low, sedimentation of nanomaterials can occur. To mitigate this, occasional recirculation of the resin ensures that particle dispersion remains homogenous during the printing process [20].

UV light scattering occurs when the refractive index of the nanomaterial and resin do not match. The degree to which light scatters through a nanocomposite resin can be lowered by selecting a resin with a refractive index that more closely resembles that of the nanomaterial. Minimizing light scattering improves the uniform curing of resin and layer adhesion [19]. Adjustments to the exposure time and photoinitiator concentration in the resin system can optimize energy absorption for more ideal nanofiller loadings. Dispersing agents like BYK additives can stabilize the nanofiller in suspension, facilitating more uniform UV light exposure of the resin during the printing process [18, 21].

Uzcategui et al. investigated the influence of photo absorbers on polymerization depth and surrounding internal stresses brought on by polymerization gradients. The presence of an exponential decay profile of polymerization across the cure depth was found to be the source of differential shrinkage responsible for surface corrugation and structural instability [22]. This finding justified further investigation into the post-curing practices like solvent soaking and thermal treatments to complete the polymerization of the resin. Figure 1 shows the exponential decay profile of polymerization gradient responsible for mechanical instability.

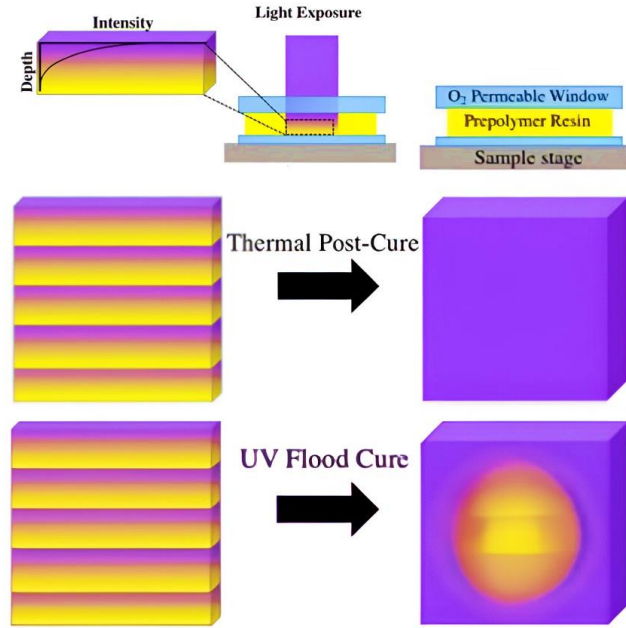


Figure 2: The polymerization gradient through resin

Hirata et al. demonstrated the effectiveness of high-aspect-ratio α -zirconium phosphate (ZrP) nanoplatelets in reducing the CTE of a bisphenol-F epoxy-based thermoset up to 40%. Despite not having a focus on SLA processes, the results support the theory behind nanomaterials lowering the CTE differential between polymers and rigid substrates. The nanoplatelet-filled epoxy, Epoxy-ZrP-TBA-MEA, is compared against a neat epoxy in Figure 2. A third formulation, Epoxy-TBA-MEA, which contains only a surfactant without nanofiller reinforcement, displays an increased CTE, suggesting that surfactant-induced plasticization negatively impacts dimensional stability [23].

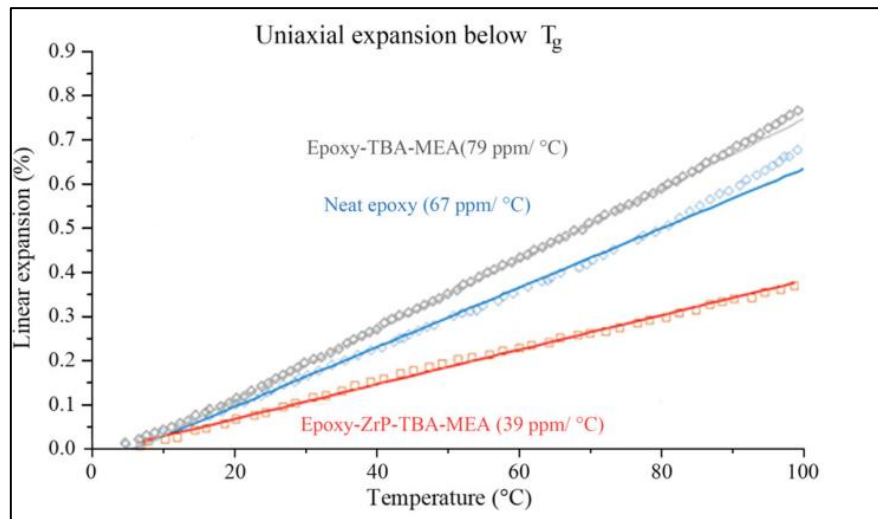


Figure 3: The uniaxial expansion below glass temperature (T_g) shows the neat epoxy (in blue) exhibiting a CTE of $67 \text{ ppm}^\circ\text{C}^{-1}$, while an epoxy formulation containing ZrP nanoplatelets (in red) [23].

By integrating these findings into SLA resin development, it becomes clear that dimensional stability is not solely dependent on polymerization control but also on how the material responds to thermal stresses post-processing. The cumulative effects of polymerization shrinkage, cure-depth gradients, and thermal expansion mismatches necessitate a multi-faceted approach to improving dimensional accuracy in SLA-printed components.

1.7 Filler-Integrated SLA Resins

Most SLA resins consist of a blend of oligomers, monomers, and photoinitiators. Adjusting the amounts of each of these constituents can be used to tune the final mechanical and thermal properties of the cured resins, and allows for careful tuning and balance of curing characteristics, mechanical performance, and printability [13, 18]. Oligomers are pre-polymerized molecular chains that serve as the primary structural components of SLA resins, often referred to as the backbone of a cured matrix, as they provide rudimentary mechanical and thermal properties.

One such oligomer that has been used in low-CTE composite resins is epoxy acrylate (EA), which is characterized by high rigidity, strength, and useful thermal stability. It is a primary component in UV-curable formulations and has successfully been combined with nanofiller additions such as silica, carbon nanotubes, and boron nitride for reducing CTE and maintaining dimensional stability during thermal cycling [17].

Sufian et al. (2024) formulated epoxy acrylate (EA)-based resins with nanofiller integration to reduce the coefficient of thermal expansion (CTE). In their approach, silica (SiO₂) nanoparticles were incorporated and thoroughly dispersed throughout the resin. The incorporation of silica nanoparticles at various concentrations improved stiffness, lowering CTE, but led to a reduction in tensile strengths of the sample, leaving the material more susceptible to fracture [17]. Brittleness poses challenges for applications requiring impact resistance and structural durability, particularly in environments subject to thermal cycling, where internal stresses may exacerbate material failure.

1.8 Inherent Brittleness of Nanocomposite Resin

The SLA photopolymerization process results in a densely crosslinked polymer network responsible for the high stiffness and strength of SLA-printed parts. This highly crosslinked structure limits polymer chain mobility, which reduces the material's ability to deform plastically, thereby increasing brittleness [24].

The post-curing process is responsible for completing polymerization and improving mechanical properties. Full conversion in polymerization often results in increased stiffness and tensile strength but at the cost of reduced ductility and toughness. This rigid crosslinked structure also increases residual stress within the material, which can lead to crack initiation and propagation under mechanical loading. Experiments on various commercial SLA resins demonstrated that elongation at failure decreased markedly after curing, with some resins showing a 50% reduction in strain before fracture [24].

The issue of brittleness is further compounded by the nature of SLA polymerization. Studies indicate that molecular architecture of the polymer network also plays a role. Research on graphene-reinforced SLA resins found that the introduction of nanofillers can alter the degree of polymerization and impact polymerization kinetics [25]

The presence of graphene oxide (GO) has been shown to interfere with light penetration during polymerization, leading to an uneven crosslinked network. This can either improve or degrade mechanical properties depending on the filler dispersion and interaction with the resin matrix [25].

Sufian et al. (2024) encountered brittleness in their MWCNT-reinforced epoxy resin formulations developed to reduce CTE. The addition of MWCNT in concentrations of 0.2 and 0.5 wt%. improved tensile strength and modulus against a neat sample [18]. Decreases in elongation observed in fracture tests clearly indicate the resin’s toughness declining with increased MWCNT concentration.

The 0.5% MWCNT-loaded resin exhibited the highest stiffness and strength but demonstrated a marked decrease in elongation at break compared to neat epoxy. This brittleness was attributed to the rigid nanotube network restricting polymer chain mobility, leading to a stiffer but more fracture-prone material. Figures 4a-d display the tensile stress-strain data for all three samples.

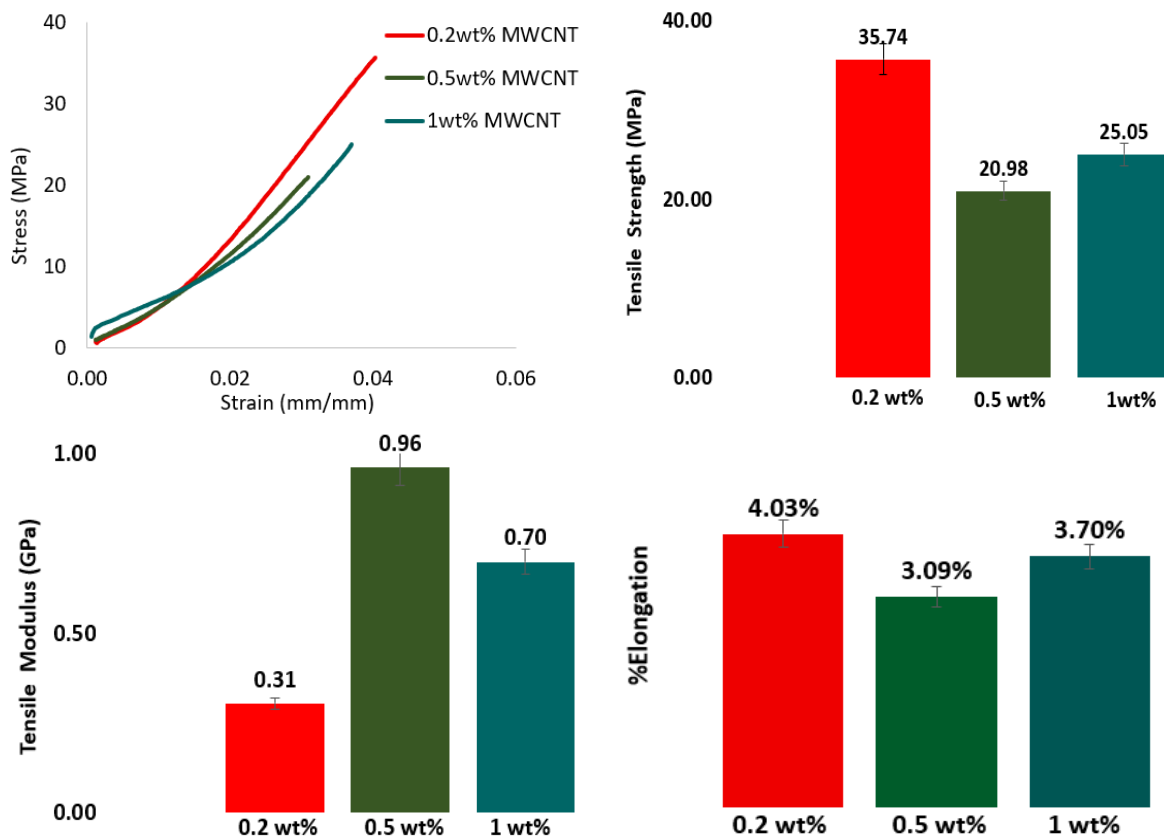


Figure 4: Stress vs strain curve, % Elongation, tensile modulus, and Tensile strength[26]

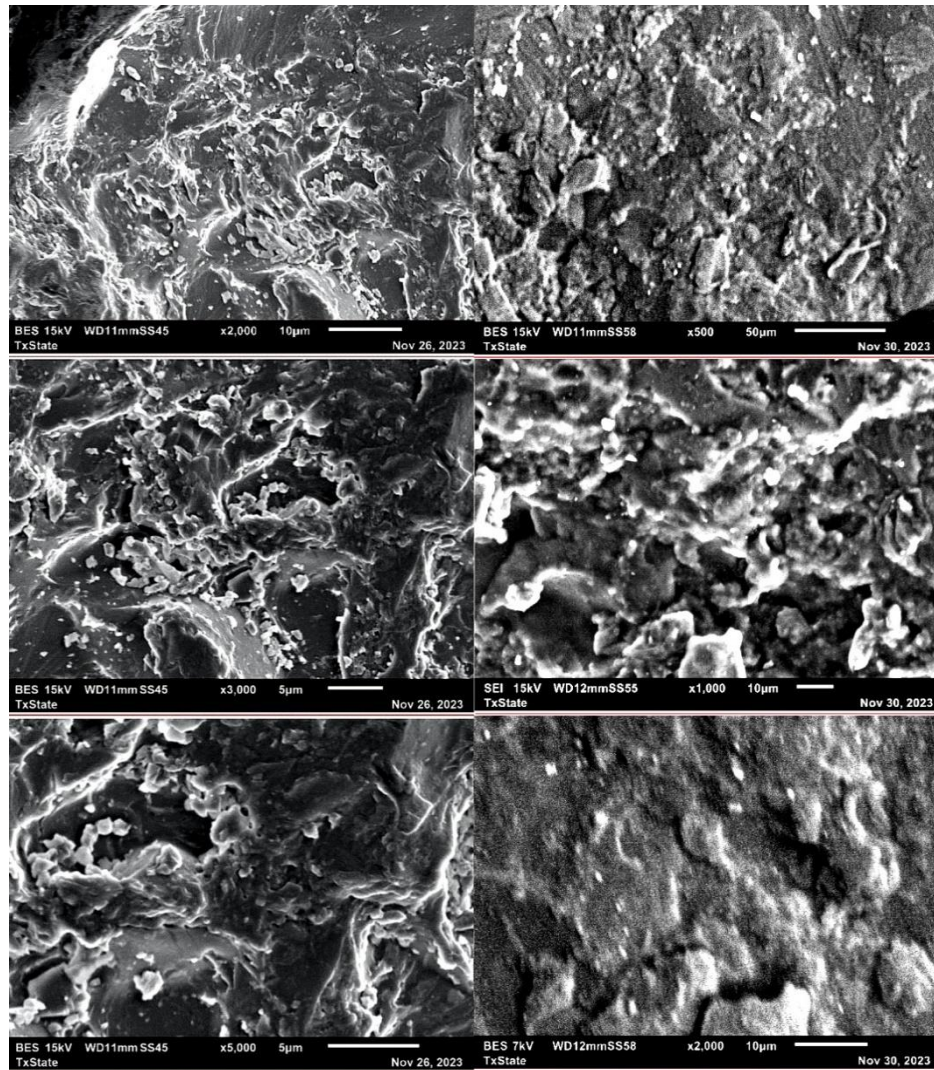


Figure 5. SEM analysis of Epoxy-Acrylate SLA Resin with MWCNT Filler

1.9 Nanostructures and Thermal Expansion

1.9.1 Effect of Nanomaterial Size on CTE

The coefficient of thermal expansion (CTE) of nanomaterials is highly dependent on their size due to the increased surface-to-volume ratio as dimensions decrease. As the particle size decreases, the fraction of atoms at the surface increases, leading to a decrease in cohesive energy, which in turn results in a higher CTE compared to bulk materials. This size-dependent effect has been observed in metals such as silver, aluminum, copper, and lead, where nanoparticles exhibit a higher volume thermal expansion coefficient than nanowires and nanofilms [27]. The relationship between size and CTE follows an inverse proportionality, with smaller nanoparticles showing more pronounced expansion effects due to their higher surface energy and lower coordination number of surface atoms [28].

Grain refinement in nanomaterials affects their thermal expansion properties. As grain size decreases, the increased grain boundary density introduces constraints on atomic vibrations,

altering phonon scattering and restricting expansion [29]. This grain-boundary-dominated behavior explains why nanostructured composites often exhibit lower CTE than their bulk counterparts. In polymer nanocomposites, including SLA resins with nanofillers, grain boundary engineering is essential to ensuring stability at the nanoscale [30].

1.9.2 Impact of Nanomaterial Shape on CTE

The shape of nanoparticles also influences their CTE, with different geometries exhibiting distinct thermal expansion behaviors. Spherical nanoparticles, due to their isotropic nature, tend to exhibit the highest CTE among different shapes, followed by nanowires and then nanofilms. This ranking can be attributed to the fraction of surface atoms exposed: spheres have the highest ratio, leading to greater lattice relaxation, while nanofilms have the least surface exposure, resulting in a more constrained expansion [27]. Theoretical expressions confirm that the thermal expansion coefficient follows the trend: spherical > nanowire > nanofilm for a given material and size [28].

2. EXPERIMENTATION

2.1 Materials

An epoxy acrylate oligomer, EBECRYL® 3700 (bisphenol A epoxy diacrylate), obtained from Allnex (Germany), was used as the base resin for all formulations. This clear, high-gloss resin possesses a viscosity of 1800–2800 mPa·s at 65.5 °C, a density of 1.18 g/cm³ at 25 °C, and a theoretical functionality of two, offering excellent UV-curing reactivity and chemical resistance. To reduce resin viscosity and increase crosslink density, trimethylolpropane triacrylate (TMPTA)—a trifunctional acrylate monomer also obtained from Allnex—was used as a reactive diluent. TMPTA is characterized by low viscosity (80–135 mPa·s at 25 °C) and is known to enhance hardness, gloss, and abrasion resistance in the final cured system.

The key reinforcing agent in this study was Silicon Carbide (SiC) Nanopowder, sourced from US Research Nanomaterials, Inc. (USA). The material consisted of beta-phase SiC nanoparticles with a reported purity of >99%, and an average particle size (APS) below 80 nm, with 0.5% of particles possibly reaching up to 100 nm. These SiC nanoparticles exhibited a grayish white color, cubic morphology, and were synthesized using a plasma-enhanced chemical vapor deposition (CVD) process. The bulk density was measured at 0.05 g/cm³, while the true density was reported as 3.216 g/cm³. The specific surface area (SSA) ranged from 25–50 m²/g, and the measured zeta potential was –27.8 mV, indicating moderately stable colloidal behavior without further surface treatment. These properties made the SiC nanopowder a suitable candidate for nanocomposite SLA formulations aimed at reducing the coefficient of thermal expansion (CTE).

Two photoinitiators—diphenyl (2,4,6-trimethylbenzoyl) phosphine oxide (TPO-L) and phenylbis(2,4,6-trimethylbenzoyl) phosphine oxide (BAPO)—were purchased from Sigma-Aldrich (USA) to initiate polymerization under UV exposure. TPO-L (C₂₂H₂₁O₂P, MW 348.37 g/mol) and BAPO (C₂₆H₂₇O₃P, MW 418.46 g/mol) were used in powder and crystalline forms, respectively, with purities exceeding 96.5% (HPLC). These initiators were chosen for their high photoreactivity and deep cure efficiency in acrylate-based systems.

All materials were used as received without further purification. Resin formulation and nanoparticle incorporation were conducted under controlled ambient conditions to ensure uniform dispersion, prevent sedimentation, and ensure formulation reproducibility across all experimental batches.

2.2 Methods

2.2.1 Resin Formulation and Preparation of Nanocomposite for SLA 3D Printing

The resin preparation process began by pre-heating the base oligomer, EBECRYL® 3700 (bisphenol A epoxy diacrylate), in a thermostatically controlled water bath at 70 °C for 30 minutes. This thermal conditioning step was implemented to reduce the oligomer's inherent high viscosity and facilitate fluid handling during formulation. After pre-heating, the required quantity of EBECRYL® 3700 was transferred into a 100 ml Pyrex beaker. Trimethylolpropane triacrylate (TMPTA), a trifunctional acrylate monomer, was then added in a predetermined ratio to act as a reactive diluent, thereby reducing viscosity and increasing the crosslinking density of the final cured network.

Following the blending of the base resin and monomer, high-purity beta-phase Silicon Carbide (SiC) nanoparticles (<80 nm, 99%+ purity, plasma CVD-synthesized) were incorporated into the resin system at target loadings of 0.2 wt%, 0.5 wt%, and 1 wt%. The SiC nanopowder exhibited a cubic morphology, a specific surface area of 25–50 m²/g, and a zeta potential of –27.8 mV, supporting stable dispersion within the liquid resin without additional surface treatments. The desired quantity of SiC was weighed and gradually introduced into the resin mixture under continuous stirring to prevent premature agglomeration.

A total of 0.50 g of photoinitiators was added to the formulation, consisting of 0.25 g each of diphenyl (2,4,6-trimethylbenzoyl) phosphine oxide (TPO-L) and phenylbis(2,4,6-trimethylbenzoyl) phosphine oxide (BAPO). These initiators were selected for their high reactivity and compatibility with acrylate-based systems, ensuring efficient photopolymerization upon UV exposure.

To achieve homogeneous dispersion of the SiC nanoparticles and eliminate potential agglomerates, the formulation was subjected to simultaneous ultrasonication and magnetic stirring. Ultrasonication was conducted using an ultrasonic processor (GEX 750 W, 20 kHz), operated at 40% amplitude and a 20% duty cycle (12 s on, 18 s off), while a magnetic stir bar maintained continuous mechanical agitation. This dual-dispersion approach was applied for a total duration of 3 hours, promoting effective deagglomeration and uniform mixing of nanoparticles throughout the resin.

After mixing, the nanocomposite resin was degassed using a THINKY ARV-310 planetary vacuum mixer (Thinky Corporation, Japan). Degassing was carried out under a 99 kPa vacuum at a mixing speed of 2000 rpm for 5 minutes to eliminate entrapped air and residual volatiles. This step ensured the formation of a defect-free matrix optimized for stereolithography-based 3D printing. All formulations were prepared under ambient laboratory conditions and stored in opaque, sealed containers to prevent premature photoactivation.

To investigate the influence of SiC nanoparticle content on the thermal and mechanical properties of the SLA resin, three distinct nanocomposite formulations were prepared with SiC loadings of 0.5 wt% and 1 wt%, respectively. Each formulation was based on a consistent 20 g quantity of EBECRYL® 3700 epoxy resin. The remaining matrix composition was adjusted by varying the amount of TMPTA to maintain suitable viscosity and flow characteristics. The photoinitiator content was held constant across all batches to ensure uniform UV-curing conditions. Table 1 summarizes the component weights used for each SiC concentration.

Components	0.5 wt% SiC	1 wt% SiC
EBECRYL 3700 BPA Epoxy Resin	20	20
Trimethylolpropane Triacrylate (TMPTA)	29.25	29.1
Phenylbis phosphine oxide (BAPO)	0.25	0.25
Diphenyl phosphine oxide (TPO-L)	0.25	0.25
Silicon Carbide Nanopowder	0.25	0.5

Table 1: Composition of SLA Resin Nanocomposites at Different Silicon Carbide Loadings

2.2.2 Fabrication of Three-Dimensional Structures by SLA 3D Printer

The fabrication of 3D structures was carried out using the Anycubic Photon D2 SLA printer, a high-resolution desktop stereolithography system employing Digital Light Processing (DLP) technology. This printer offers a build volume of $131 \times 73 \times 165$ mm, with an XY resolution of $51 \mu\text{m}$ and a native resolution of 2560×1440 pixels, ensuring exceptional print accuracy and surface finish. The integrated DLP light engine has a projected lifespan of up to 20,000 hours, making it highly durable for extended use. The printing parameters, specifically exposure times, were optimized for each nanosilica loading to account for variations in optical density and resin viscosity. These exposure settings—including both burn-in and normal layer curing times—are summarized in Table 2. All models were sliced using Lychee Slicer software, which allowed fine-tuned control of exposure, lift speeds, and support generation. After printing, the fabricated parts were detached from the build platform and washed in isopropyl alcohol (IPA) to remove any residual uncured resin. Post-processing included UV post-curing to enhance crosslinking and mechanical performance. Tensile and flexural specimens were printed in accordance with ASTM D638 and ASTM D790 standards, respectively, ensuring consistency and reliability in subsequent mechanical testing.

SiC Loading (wt%)	Burn-in Layer Exposure Time (s)	Normal Layer Exposure Time (s)
0.5	25	18
1	100	70

Table 2: Exposure parameters for SLA printing at varying Silicon Carbide loading levels

2.3 Characterization.

2.3.1 Mechanical Properties

The tensile properties of both the neat resin and the nanocomposite resin were evaluated using an MTS Exceed Series 40 Electromechanical Testing System, manufactured by MTS Systems. The tensile specimens were printed according to the ASTM D638 "Standard Test Method for Tensile Properties of Plastics," specifically using Type IV geometry. The overall sample dimensions were 115 mm in length, with a narrow section width of 6 mm and a thickness of 3.2 mm. Tensile testing was conducted at a strain rate of 0.2 inches per minute, and the gauge length of the specimens was accurately measured using a digital slide caliper to ensure precise data collection.

The flexural properties of the neat resin and nanocomposite resin were tested using a UTS Electromechanical Test System, manufactured by UnitedTest in Beijing, China. The specimens were printed following ASTM D790 "Standard Test Method for Flexural Properties of Unreinforced and Reinforced Plastics and Electrical Insulating Materials." Each sample measured 125 mm in length, 12.7 mm in width, and 3.2 mm in thickness. Flexural testing was carried out at a strain rate of 0.2 inches per minute, with the gauge length of the specimens precisely measured using a digital slide caliper to ensure accuracy in the data collection process.

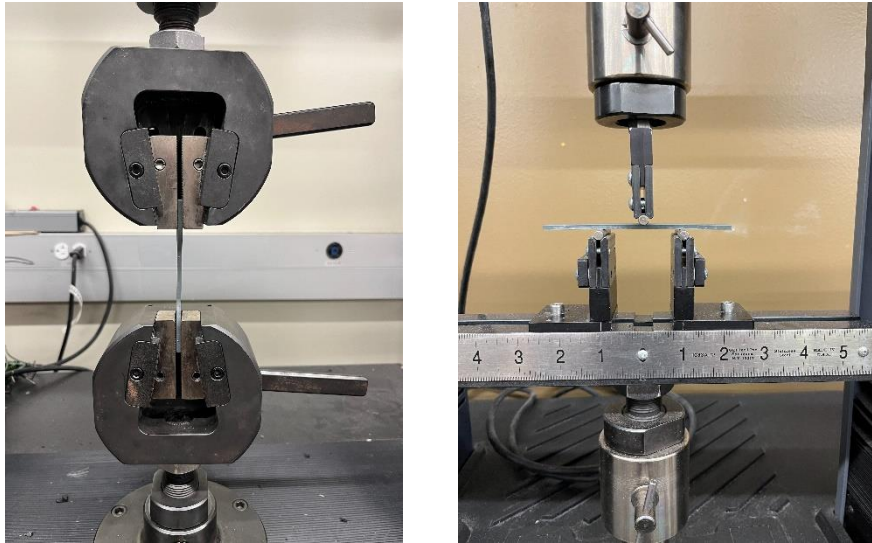


Figure 6: Tensile testing via United Testing System (UTS) setup (left), 3-point bend test via Material Testing System (MTS)(right)

2.3.2 Thermal Properties

The thermo-mechanical properties of the neat Ebecryl resin and the Silicon Carbide (SiC) infused resin were analyzed using Dynamic Mechanical Analysis (DMA) with the TMA Q400 System from TA Instruments (New Castle, Delaware, USA) in macro expansion mode. The testing was conducted over a temperature range from 30 °C to 150 °C, with a heating rate of 5 °C per minute, and a frequency of 0.5 Hz. The thermo-mechanical analysis was performed following the guidelines of ASTM E831-19, "Standard Test Method for Linear Thermal Expansion of Solid Materials by Thermomechanical Analysis," ensuring accurate measurement of thermal expansion behavior across the specified temperature range.

The mean coefficient of thermal expansion (CTE) was calculated using the following equation as per ASTM E831-19:

$$\alpha_m = \frac{\Delta L_{sp} \times k}{L \times \Delta T}$$

where:

- α_m = mean coefficient of linear thermal expansion, $\mu\text{m}/(\text{m}\cdot^\circ\text{C})$,
- k = calibration coefficient, from Test Method E2113,
- L = specimen length at room temperature, m,
- ΔL_{sp} = change of specimen length, μm ,
- ΔT = temperature difference over which the change in specimen length is measured, $^\circ\text{C}$,
- T = midpoint temperature of the temperature range ΔT



Figure 7: Mounted CTE sample on the TA Instruments TMA Q400

3. RESULTS

3.1 Scanning Electron Microscopy (SEM)

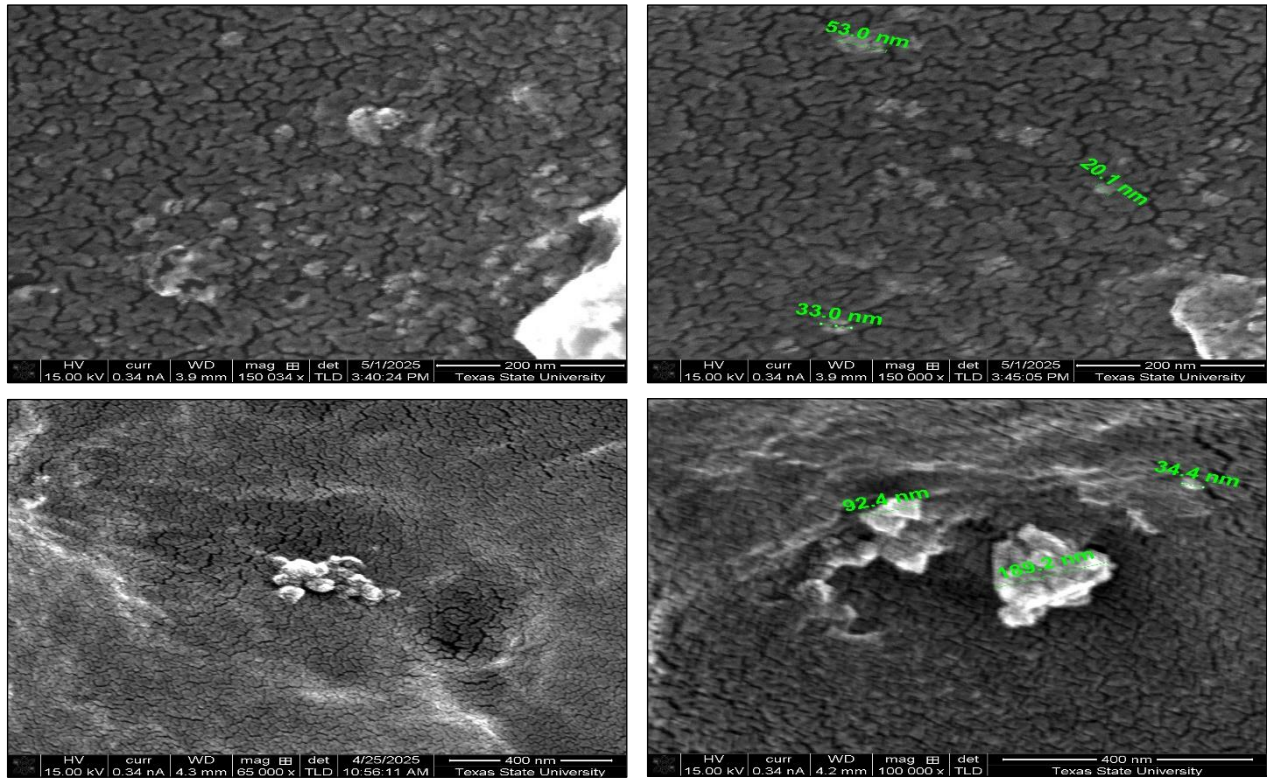


Figure 8: SEM images for 0.5 wt% SiC (top) and 1 wt% SiC (bottom)

The morphology of the SiC-reinforced Ebecryl resin composites was analyzed using Scanning Electron Microscopy (SEM) for both 0.5 wt% and 1 wt% SiC loading levels. The SEM micrographs (Figure Xa–Xd) reveal the distribution and dispersion quality of SiC nanoparticles within the cured polymer matrix.

For the 0.5 wt% SiC sample (Figure Xa and Xb), the particles appear to be well dispersed throughout the matrix with minimal visible agglomeration. The particles are relatively evenly spaced, and there is no evidence of significant clustering or sedimentation. This indicates effective mixing and sufficient interfacial bonding between the SiC fillers and the resin, likely facilitated by proper surface energy matching and processing parameters.

At the 1 wt% SiC loading level (Figure Xc and Xd), a largely uniform dispersion is still maintained. However, a few regions show minor agglomeration of SiC particles. These clusters are relatively small and sparse, suggesting that while particle interaction increases slightly with higher loading, the dispersion quality remains acceptable and does not significantly compromise the composite's uniformity.

Overall, the SEM analysis confirms that the incorporation of SiC nanoparticles at both 0.5 wt% and 1 wt% results in a generally homogeneous microstructure with good particle dispersion.

This uniformity is critical for achieving consistent mechanical and thermal properties throughout the printed parts.

3.2 Tensile Properties

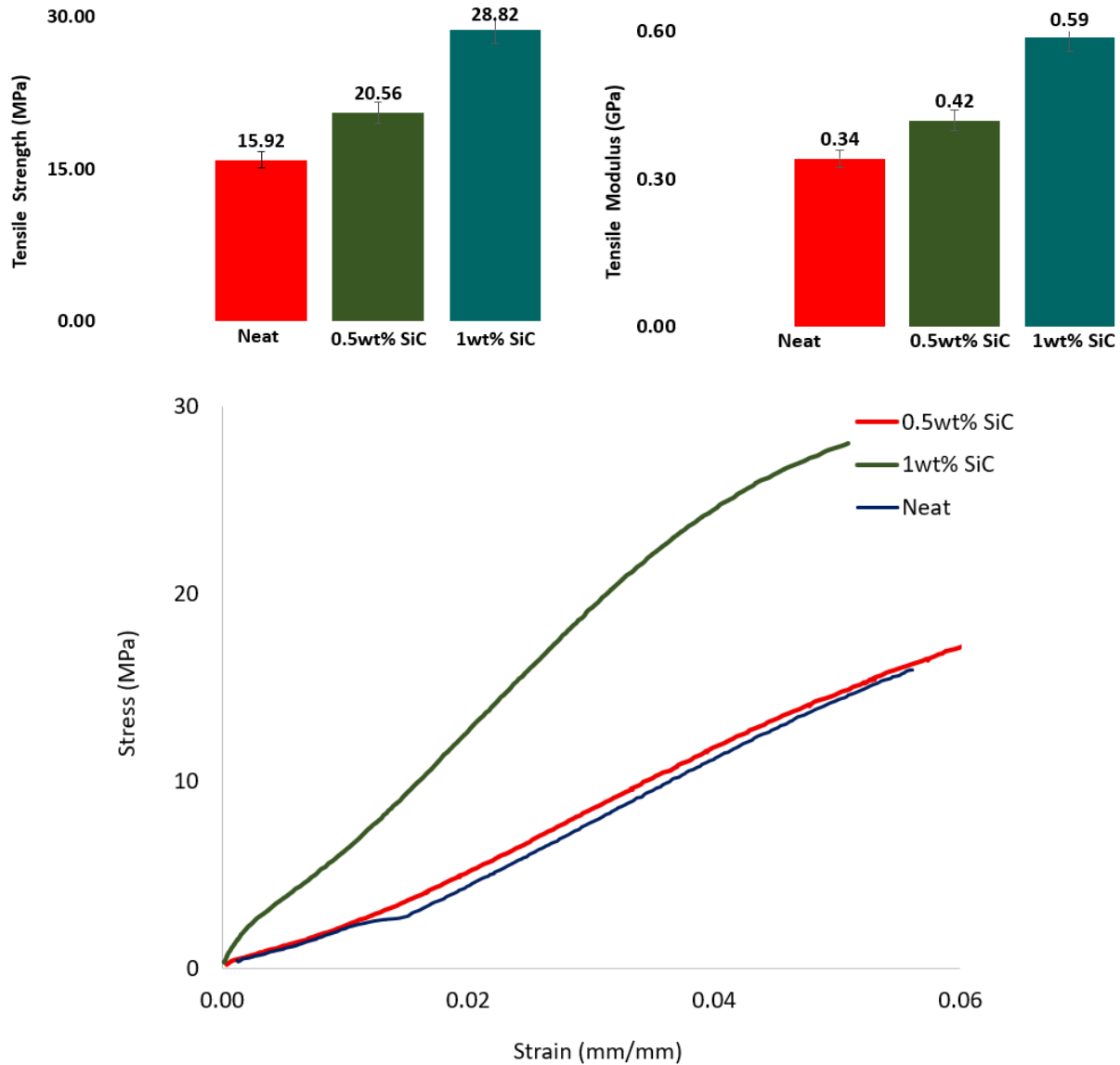


Figure 9: Comparison of tensile strength, modulus and stress vs strain curve between Ebecryl Neat, 0.5wt% and 1wt% loading levels of SiC

Tensile testing was conducted to evaluate the effect of silicon carbide (SiC) nanoparticle reinforcement on the mechanical performance of the Ebecryl resin. The two key parameters considered were the Ultimate Tensile Strength (UTS) and the Tensile Modulus, as presented in Figure 9.

The UTS of the neat Ebecryl formulation was measured at 15.92 MPa. Upon incorporating 0.5 wt% SiC, the tensile strength decreased to 13.42 MPa, suggesting that a small addition of particles may lead to slight weakening due to stress concentrators or insufficient load transfer at low filler content. However, a significant increase in UTS was observed at 1 wt% SiC, reaching 28.82 MPa, which represents an improvement of over 80% compared to the neat resin. This enhancement can be attributed to better interfacial adhesion and effective load transfer between the well-dispersed SiC particles and the matrix at this loading level.

In terms of stiffness, the tensile modulus of the neat Ebecryl was 342.1 MPa. The modulus remained nearly unchanged at 339.2 MPa for the 0.5 wt% SiC formulation, indicating that the reinforcement effect was not significant at this lower concentration. However, at 1 wt% SiC, the modulus sharply increased to 572.9 MPa, confirming substantial stiffening of the resin matrix due to the presence of rigid ceramic particles.

These results suggest that while a low filler concentration may not substantially alter tensile properties or may even cause degradation, an optimized filler loading (in this case, 1 wt%) can markedly improve both strength and stiffness. The findings align with the morphological observations, where particle dispersion remained relatively uniform even at 1 wt%, minimizing agglomeration-induced defects.

3.3 Flexural Properties

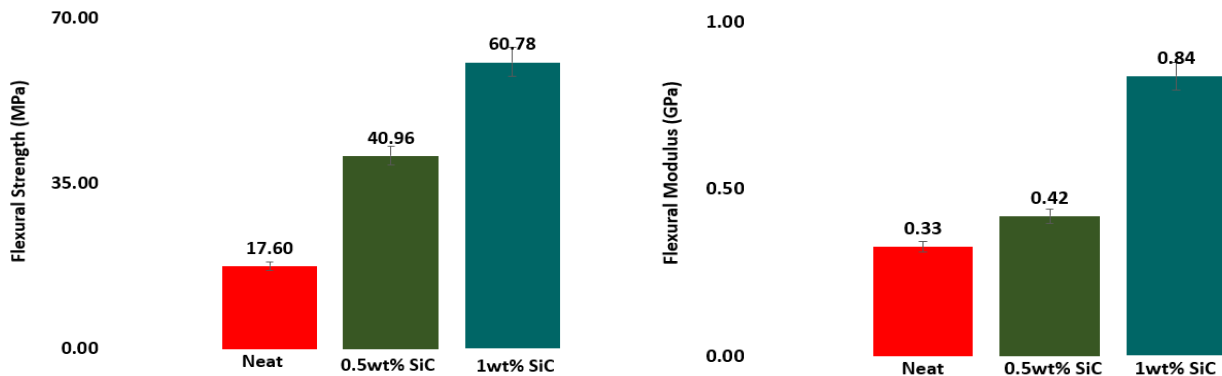


Figure 10: Comparison of flexural strength, flexural modulus and load vs deflection curve between Ebecryl Neat, 0.5 wt% and 1 wt% loading levels of SiC

Flexural strength and modulus were evaluated to assess the bending performance of the SiC-reinforced Ebecryl resin composites. As presented in the figures, both properties showed significant variation with different loading levels of SiC nanoparticles.

The neat Ebecryl resin exhibited a flexural strength of 17.20 MPa. With the addition of 0.5 wt% SiC, a slight decrease in flexural strength to 15.18 MPa was observed. This reduction might be attributed to early-stage particle clustering or insufficient interfacial bonding, which can introduce weak points under bending stress. However, at 1 wt% loading, the flexural strength

dramatically increased to 47.08 MPa, indicating a strong reinforcing effect of the ceramic filler when uniformly dispersed and sufficiently interacting with the resin matrix.

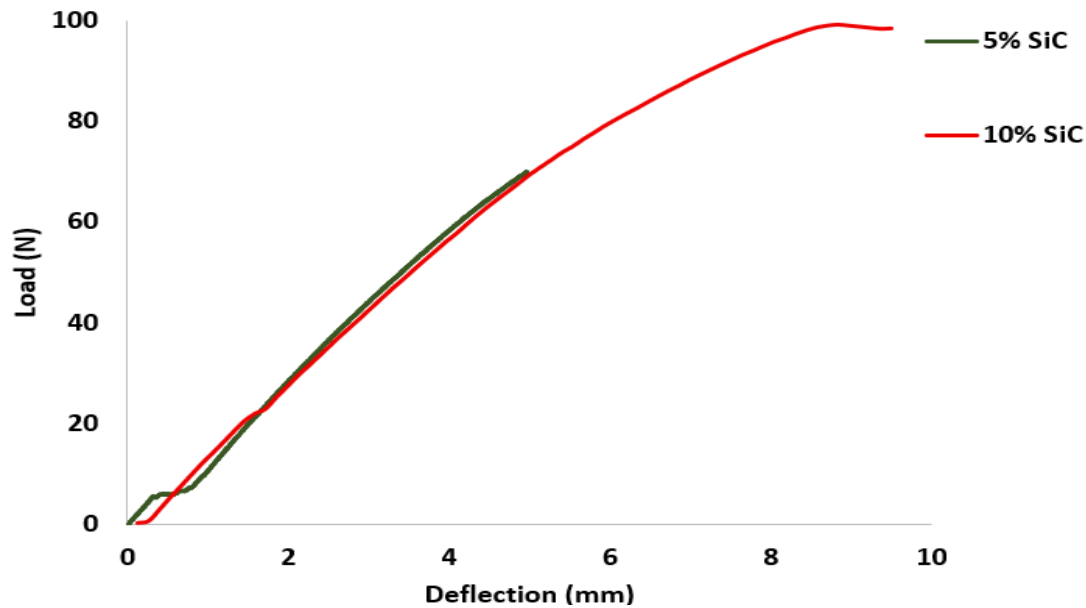


Figure 11: Load vs deflection curve for 0.5wt% and 1wt% SiC

A similar trend was observed for the flexural modulus. The modulus for the neat resin was 298.3 MPa, which remained nearly unchanged at 291.1 MPa for the 0.5 wt% SiC formulation. In contrast, the 1 wt% SiC sample exhibited a substantial increase in modulus to 941.1 MPa, reflecting a threefold enhancement in stiffness. This is a clear indication of improved resistance to deformation under flexural loads due to the presence of rigid, load-bearing SiC particles.

These results reinforce the earlier morphological observations: at higher loading levels, SiC particles enhance structural integrity and load-bearing capacity without compromising dispersion. The sharp improvement in both strength and stiffness at 1 wt% suggests it is an optimal formulation for mechanical reinforcement in SLA-printed nanocomposites.

3.4 Thermo-Mechanical Analysis

Thermal expansion behavior of the SiC-reinforced resin composites was evaluated using Thermomechanical Analysis (TMA). As shown in the figure, the dimensional change of each specimen with increasing temperature was recorded and compared across neat Ebecryl resin, 0.5 wt% SiC, and 1 wt% SiC formulations.

The neat Ebecryl resin exhibited the highest dimensional change with increasing temperature, indicating a relatively high coefficient of thermal expansion (CTE). Incorporation of SiC nanoparticles significantly reduced thermal expansion. The 0.5 wt% SiC sample demonstrated the lowest dimensional growth across the temperature range, suggesting that a small amount of well-dispersed ceramic filler can effectively constrain thermal mobility in the polymer matrix.

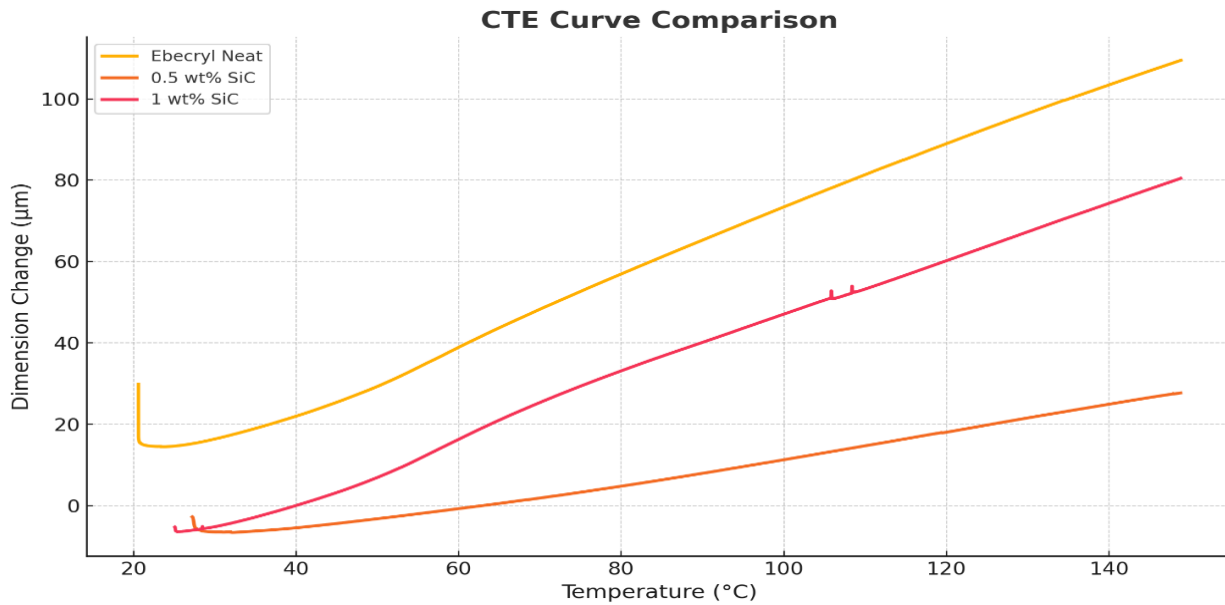


Figure 11: Comparison of Coefficient of thermal expansion between Ebecryl Neat, 0.5wt% and 1wt% loading levels of SiC

Interestingly, the 1 wt% SiC sample displayed a moderate reduction in expansion compared to the neat resin but exhibited higher dimensional change than the 0.5 wt% formulation. This may be attributed to slight particle agglomeration at higher filler content, which can lead to localized stress relaxation or interfacial debonding under thermal loading, thereby reducing the efficiency of thermal constraint.

The results demonstrate that adding SiC fillers lowers the CTE of the photopolymer resin, with the 0.5 wt% SiC providing the most effective thermal stability in terms of dimensional control. This reduction is crucial for high-precision SLA applications where thermal distortion must be minimized.

4. CONCLUSIONS

This study demonstrated the successful formulation and evaluation of a silicon carbide (SiC) nanoparticle-reinforced epoxy acrylate resin system for stereolithography (SLA) applications. By incorporating SiC nanoparticles at loadings of 0.5 wt% and 1 wt%, the influence of nanofiller content on morphology, mechanical behavior, and thermal expansion characteristics of the printed composites was systematically investigated.

Scanning Electron Microscopy (SEM) confirmed effective nanoparticle dispersion across both loading levels. The 0.5 wt% formulation showed highly uniform distribution with negligible agglomeration, while the 1 wt% sample maintained acceptable dispersion with only minor, isolated clusters. This microstructural uniformity is critical for ensuring consistent mechanical performance and dimensional stability in 3D-printed parts.

Mechanical testing revealed a clear dependence of tensile and flexural properties on the SiC loading level. Although the 0.5 wt% SiC composite showed a slight reduction in both tensile and flexural strength—likely due to stress concentrators or early-stage particle clustering—the 1 wt% SiC formulation achieved significant reinforcement. The tensile strength increased by over 80% and the flexural strength by nearly 175% relative to the neat resin. Likewise, stiffness (as measured by tensile and flexural modulus) exhibited substantial enhancement, particularly at 1 wt%, highlighting the load-bearing capacity imparted by the ceramic filler.

Thermal analysis via Thermomechanical Analysis (TMA) demonstrated that SiC incorporation effectively reduced the coefficient of thermal expansion (CTE) of the composite. Interestingly, the 0.5 wt% SiC sample achieved the lowest CTE, indicating optimal thermal constraint due to uniform dispersion and strong interfacial bonding. While the 1 wt% sample still outperformed the neat resin in terms of thermal stability, the slightly increased expansion was attributed to minor agglomeration, which may have introduced localized stress relaxation under thermal loading.

In summary, SiC nanoparticle reinforcement enhances the mechanical and thermal performance of SLA resins, but the effect is highly sensitive to filler concentration and dispersion quality. The 1 wt% formulation demonstrated optimal mechanical performance, whereas the 0.5 wt% formulation provided superior thermal stability. These findings suggest that tailored nanofiller concentrations can be strategically selected based on the specific performance requirements of SLA-printed components—whether for structural load-bearing applications or for high-precision parts requiring dimensional accuracy under thermal stress.

The successful integration of SiC into a photopolymer matrix without significant sedimentation or loss of print fidelity presents a promising path forward for expanding the functional scope of SLA resins in aerospace, electronics, and high-temperature polymer applications. Future work may explore surface functionalization of SiC to further enhance interfacial bonding, and extend the investigation to multi-filler hybrid systems for simultaneous mechanical, thermal, and electrical enhancements.

5. REFERENCES

- [1] T. R. Mhmood and N. K. Al-Karkhi, "A Review of the Stereo lithography 3D Printing Process and the Effect of Parameters on Quality," *Al-Khwarizmi Engineering Journal*, vol. 19, no. 2, pp. 82-94, 2023.
- [2] J. Huang, Q. Qin, and J. Wang, "A review of stereolithography: Processes and systems," *Processes*, vol. 8, no. 9, p. 1138, 2020.
- [3] M. Jiménez, L. Romero, I. A. Domínguez, M. d. M. Espinosa, and M. Domínguez, "Additive manufacturing technologies: an overview about 3D printing methods and future prospects," *Complexity*, vol. 2019, no. 1, p. 9656938, 2019.
- [4] G. R. Pereira, F. Gasi, and S. R. Lourenço, "Review, analysis, and classification of 3D printing literature: types of research and technology benefits," *Int. J. Adv. Eng. Res. Sci*, vol. 6, no. 6, pp. 167-187, 2019.
- [5] D. Kam, O. Rulf, A. Reisinger, R. Lieberman, and S. Magdassi, "3D printing by stereolithography using thermal initiators," *Nature Communications*, vol. 15, no. 1, p. 2285, 2024. [Online]. Available: <https://www.nature.com/articles/s41467-024-46532-0.pdf>.
- [6] J. Novotny *et al.*, "Advantages of stereolithographic 3D printing in the fabrication of the Affiblot device for dot-blot assays," *Microchimica Acta*, vol. 191, no. 8, p. 442, 2024. [Online]. Available: https://pmc.ncbi.nlm.nih.gov/articles/PMC11219379/pdf/604_2024_Article_6512.pdf.
- [7] M. A. Mustafa *et al.*, "A Comparative Review of 3D Printing Technologies and their Applications: A Systematic Review for Future of Medicine Fabrication," 2025.
- [8] C. I. Higgins, T. E. Brown, and J. P. Killgore, "Digital light processing in a hybrid atomic force microscope: In Situ, nanoscale characterization of the printing process," *Additive manufacturing*, vol. 38, p. 101744, 2021.
- [9] J. Cheng, S. Yu, R. Wang, and Q. Ge, "Digital light processing based multimaterial 3D printing: challenges, solutions and perspectives," *International Journal of Extreme Manufacturing*, vol. 6, no. 4, p. 042006, 2024.
- [10] S. Mubarak *et al.*, "Enhanced mechanical and thermal properties of stereolithography 3D printed structures by the effects of incorporated controllably annealed anatase TiO₂ nanoparticles," *Nanomaterials*, vol. 10, no. 1, p. 79, 2020. [Online]. Available: https://mdpi-res.com/d_attachment/nanomaterials/nanomaterials-10-00079/article_deploy/nanomaterials-10-00079-v2.pdf?version=1579422333.
- [11] B. Susanto *et al.*, "Investigating Microstructural and Mechanical Behavior of DLP-Printed Nickel Microparticle Composites," *Journal of Composites Science*, vol. 8, no. 7, p. 247, 2024.
- [12] D. Dubey, A. S. Mirhakimi, and M. A. Elbestawi, "Negative thermal expansion metamaterials: a review of design, fabrication, and applications," *Journal of Manufacturing and Materials Processing*, vol. 8, no. 1, p. 40, 2024.
- [13] C. Hammond, J. Greenstreet, W. Gomez, R. Dang, and J. Tate, "Development of a Low Thermal Expansion Sla Resin for Nickel Plating Applications," 2022.
- [14] R. R. S. Muhammad A. Sufian, Wasi Shadman, Ibrahim K. Tanim, Benicia Cooper, Jitendra Tate, "Development of a Low Thermal Expansion Nanocomposite Resin for MSLA 3D Printer," in *SAMPE 2024*, 2024 2024: NA SAMPE, 2024, p. 19, doi: 10.33599/nasampe/s.24.0229. [Online]. Available:

https://digitallibrarynasampe.org/data/webpages/s2024_webpages/TP24-0000000229.html

- [15] M. A. Sufian, R. R. Sheley, and J. Tate, "Photocurable SLA Resin Formulation for Reduced Coefficient of Thermal Expansion," in *2024 International Solid Freeform Fabrication Symposium*, Austin, Texas, J. J. Beaman, D. Kovar, M. Cullinan, Z. Sha, R. Crawford, and M. Tilton, Eds., 2024, vol. 35: University of Texas at Austin, doi: 10.26153/tsw/58091. [Online]. Available: <https://hdl.handle.net/2152/130743>
- [16] A. Saboori, S. K. Moheimani, M. Pavese, C. Badini, and P. Fino, "New nanocomposite materials with improved mechanical strength and tailored coefficient of thermal expansion for electro-packaging applications," *Metals*, vol. 7, no. 12, p. 536, 2017.
- [17] M. A. Sufian, R. R. Sheley, and J. Tate, "PHOTOCURABLE SLA RESIN FORMULATION FOR REDUCED COEFFICIENT OF THERMAL EXPANSION," 2023.
- [18] M. A. Sufian, R. R. Sheley, W. Shadman, I. K. Tanim, B. Cooper, and J. Tate, "Development of a Low Thermal Expansion Nanocomposite Resin for MSLA 3D Printer," *SAMPE 2024*, 2024.
- [19] G. Fei *et al.*, "Photocurable resin-silica composites with low thermal expansion for 3D printing microfluidic components onto printed circuit boards," *Materials Today Communications*, vol. 31, p. 103482, 2022.
- [20] J. Hector Sandoval and R. B. Wicker, "Functionalizing stereolithography resins: effects of dispersed multi-walled carbon nanotubes on physical properties," *Rapid Prototyping Journal*, vol. 12, no. 5, pp. 292-303, 2006.
- [21] K. H. Ahmad, Z. Mohamad, Z. I. Khan, and M. Habib, "Tailoring UV Penetration Depth in Photopolymer Nanocomposites: Advancing SLA 3D Printing Performance with Nanofillers," *Polymers*, vol. 17, no. 1, p. 97, 2025, doi: 10.3390/polym17010097.
- [22] A. C. Uzcategui, A. Muralidharan, V. L. Ferguson, S. J. Bryant, and R. R. McLeod, "Understanding and improving mechanical properties in 3D printed parts using a dual-cure acrylate-based resin for stereolithography," *Advanced engineering materials*, vol. 20, no. 12, p. 1800876, 2018. [Online]. Available: <https://pmc.ncbi.nlm.nih.gov/articles/PMC6370025/pdf/nihms-1004424.pdf>.
- [23] T. Hirata, P. Li, F. Lei, S. Hawkins, M. J. Mullins, and H. J. Sue, "Epoxy nanocomposites with reduced coefficient of thermal expansion," *Journal of Applied Polymer Science*, vol. 136, no. 26, p. 47703, 2019.
- [24] C. Riccio *et al.*, "Effects of curing on photosensitive resins in SLA additive manufacturing," *Applied Mechanics*, vol. 2, no. 4, 2021.
- [25] S. L. de Armentia, R. Giménez, J. del Real, B. Serrano, J. Cabanelas, and E. Paz, "Effect of graphene and graphene oxide addition on crosslinking and mechanical properties of photocurable resins for stereolithography," *International Journal of Bioprinting*, vol. 10, no. 6, p. 4075, 2024.
- [26] M. A. Sufian, R. R. Sheley, and J. Tate, "Photocurable SLA Resin Formulation for Reduced Coefficient of Thermal Expansion," presented at the 2024 International Solid Freeform Fabrication Symposium, University of Texas, Austin, Texas, USA, 2024. [Online]. Available: <https://repositories.lib.utexas.edu/items/048427f6-c23a-487c-b42c-540e273bb08e>.

- [27] R. L. Jaiswal, B. K. Pandey, D. Mishra, and H. Fatma, "Thermo-physical Behavior of Nanomaterials with the Change in Size and Shape," *International Journal of Thermodynamics*, vol. 24, no. 1, pp. 1-7, 2021.
- [28] M. Singh and M. Singh, "Impact of size and temperature on thermal expansion of nanomaterials," *Pramana*, vol. 84, pp. 609-619, 2015.
- [29] Q. Wu, W.-s. Miao, Y.-d. Zhang, H.-j. Gao, and D. Hui, "Mechanical properties of nanomaterials: A review," *Nanotechnology Reviews*, vol. 9, no. 1, pp. 259-273, 2020.
- [30] K. Takenaka, "Negative thermal expansion materials: technological key for control of thermal expansion," *Science and technology of advanced materials*, vol. 13, no. 1, p. 013001, 2012. [Online]. Available: <https://pmc.ncbi.nlm.nih.gov/articles/PMC5090290/pdf/TSTA11661035.pdf>.